Bulletin of Geophysics and Oceanography Vol. 65, n. 2, pp. 241-256; June 2024
DOI 10.4430/bgo00449

A laboratory multisensor geophysical approach for monitoring steel rebar corrosion in concrete structures

G. Fornasari[1,2] and E. Rizzo[1,2]

[1] *Department of Physics and Earth Science, University of Ferrara, Ferrara, Italy*
[2] *Institute of Methodologies for Environmental Analysis, National Research Council, Tito Scalo (PZ), Italy*

(Received: 23 May 2023; accepted: 20 December 2023; published online: 5 April 2024)

ABSTRACT Non-destructive monitoring methods are crucial for the management and maintenance of assets, which include reinforced concrete (RC) structures. Steel reinforcing bar (rebar) corrosion is one of the main causes of deterioration of engineered reinforced structures as it decreases their strength and serviceability. The purpose of this study was to use non-destructive geophysical techniques to detect and monitor rebar corrosion phenomena. To achieve this, several laboratory tests were performed on RC samples partially immersed in water containing a 5% of sodium chloride (NaCl) solution. Moreover, an accelerated corrosion phenomenon was produced by supplying direct current power along the rebar. Ground-penetrating radar measurements were performed on the concrete surface using 2.0 GHz centre frequency antennas, self-potential acquisitions, and electrical resistivity tomography. Even though each technique provided specific information, a data integration approach, simultaneously using different sensors, would further improve the overall quality of the diagnosis. The data set collected was used for an integrated detection approach, effective in observing the evolution of the corrosion process along the reinforcement bar. Through these laboratory results, a multisensor approach and an integrated observation proved useful for observing the evolution of corrosion phenomenon in reinforcement bars, as a consequence of the steel rebar corrosion.

Key words: rebar corrosion monitoring, reinforced concrete, non-destructive testing, ground-penetrating radar, self-potential, mini-electrical resistance tomography.

1. Introduction

Concrete is one of the most common and popular construction materials due to its high durability, waterproofness, plasticity, and relatively affordable prices (Venkatesan *et al*., 2003; Pacheco-Torgal *et al*., 2018; Robles *et al*., 2022). However, concrete in buildings and civil infrastructures is susceptible to deterioration caused by various sources such as, for example, mechanical degradation induced by shocks, erosion, settlement, structural overloads, or physical degradation due to freeze-thaw cycles, thermal variations or chemical degradation (i.e. alkali-silica reaction, acid attacks, exposure to high temperatures). Among these, the corrosion of embedded steel reinforcing bars (rebars) is reported to be the primary cause of concrete deterioration in reinforced concrete (RC) structures (Robles *et al*., 2022). Steel rebar corrosion creates enormous economic loss (Ramezanianpour *et al*., 2011), reduces

service life and durability of the structures, and puts user safety at risk. To guarantee safety, compliance with an appropriate design and construction of the materials is essential as it takes into consideration the fact that building materials are subject to deterioration over time. The annual maintenance costs, imputable to corrosion phenomenon, are over 3% of the world gross domestic product (Ormellese *et al*., 2006). Steel rebar corrosion, in RC, can be defined through multiple phases, starting from corrosion initiation, rust propagation, and corrosion acceleration. When RC structures are built, the high alkalinity of the concrete (i.e. pH 12~13) produces a thin passive layer (i.e. iron oxide film, Fe_2O_3), which covers the reinforcing steel in sound concrete, thus, significantly reducing the corrosion rate (Robles *et al*., 2022). When either the concrete pH decreases, and reaches a certain level, or the concrete chloride ion concentration exceeds the specific threshold, the protective layer becomes unstable (Ormellese *et al*., 2006; Ramezanianpour *et al*., 2011; Daniyal and Akhtar, 2020; Tuutti *et al*., 2020; Robles *et al*., 2022). An unstable and damaged passive layer of the steel reinforcement causes the initiation and progression of corrosion in steel. The oxidation of metallic iron causes a 600% increase in the volume of the original iron (Duffó *et al*., 2012).

The volume increase enhances the formation of microcracks and internal voids (Daniyal and Akhtar, 2020), which, in turn, increase concrete permeability, thus accelerating moisture penetration. When neglected, this can result in serious damage to concrete, which can lead to further deterioration of the RC structural elements (Robles *et al*., 2022). When the first cracks appear on the concrete surface, corrosion has generally reached an advanced stage, and maintenance action is immediately required (Bossio *et al*., 2015; Fornasari *et al*., 2023). A reliable inspection method is, therefore, essential at an early stage, i.e. before the functionality of the RC structure is seriously damaged by steel rebar corrosion (Zaki *et al*., 2015; Fornasari *et al*., 2023).

The early detection of rebar corrosion in bridges, tunnels, buildings, and other RC civil engineering structures is important to reduce the expensive cost involved in repairing the deteriorated structure, planning the maintenance activities, and preparing effective monitoring plans that guarantee knowledge of the state of health of the investigated structures.

One of the most promising approaches, which can be adopted to delay the degradation of existing structures, is the extensive use of non-destructive testing (NDT) methods (Tešic' *et al*., 2021; Fornasari *et al*., 2023). In the field of engineering, NDT methods are currently widely applied to investigate RC elements of civil structures and infrastructures (Verma *et al*., 2014; Capozzoli and Rizzo, 2017; Tosti *et al*., 2020; Capozzoli *et al*., 2021; Fornasari *et al*., 2022). The high resolution and repeatability of such methods, together with analyses based on the study of variations of physical properties, enable identifying defects and fractures caused by induced stresses, intrinsic inhomogeneities, or structural problems. From this perspective, the use of NDT methods, and the progress made in recent years in visualising the results obtained with such methods, will lead to an increased use of advanced NDT methods in the future (Tosti *et al*., 2020; Capozzoli *et al*., 2021; Fornasari *et al*., 2022). Measuring the free corrosion potential [i.e. self-potential (SP)] of steel reinforcements on the concrete surface is one of the earliest methods for assessing the corrosion condition of RC (Hornbostel *et al*., 2013). This method has been adopted as a standard in a number of countries, and is widely used (Shevtsov *et al*., 2022). The use of combined and integrated NDT techniques is important for inspection, as it overcomes the limitation of measuring instantaneous corrosion rates and improves estimation of the service life of RC structures. In fact, NDT and rebar corrosion evaluation are major factors in predicting the service life of RC structures.

Recent studies define the benefits in combining several NDT methods for monitoring steel rebar corrosion of RC laboratory samples (Bossio *et al*., 2015; Robles *et al*., 2022; Fornasari *et al*., 2023). Moreover, various methods for accelerating reinforcement corrosion in a concrete

structure have been used by several researchers (Ramezanianpour *et al*., 2011; Bossio *et al*., 2015; Capozzoli and Rizzo, 2017; Tosti *et al*., 2020; Capozzoli *et al*., 2021; Tešic' *et al*., 2021; Fornasari *et al*., 2023).

In this paper, geophysical acquisitions were made before, during, and after an accelerated laboratory corrosion test. In the last decade, only a few studies have exploited ground-penetrating radar (GPR) to observe steel rebar corrosion in the laboratory (Hubbard *et al*., 2003; Hornbostel *et al*., 2013; Hong *et al*., 2014, 2015; Verma *et al*., 2014; Bossio *et al*., 2015; Zaki *et al*., 2015; Ohtsu, 2016; Tešic' *et al*., 2021; Fornasari *et al*., 2022, 2023; Shevtsov *et al*., 2022) and in the field (Lai *et al*., 2013; Chang *et al*., 2022; Tešic' *et al*., 2022). For this reason, it is fundamental to establish the influence that the corrosion process exerts on the GPR signal with accurate laboratory tests (Robles *et al*., 2022; Fornasari *et al*., 2023). All these studies on the use of GPR for rebar corrosion investigation address the qualitative detection of corrosion. Nevertheless, a quantitative non-destructive approach, aimed at estimating rebar corrosion in existing concrete, would be significantly useful in estimating the time required to monitor the service life of each RC structure (Fornasari *et al*., 2023). This paper presents new controlled laboratory tests which focus on the analysis of GPR signals, electrical resistivity tomography (ERT), and SP data changes as consequences of corrosion. In detail, the GPR data were processed and analysed by taking into account the signal envelope attribute (Hilbert Transform) applied to A-scan amplitude data. Moreover, to evaluate quality control and assess the durability of concrete structures, particular attention has been paid to electrical resistivity measurement techniques. The electrical resistivity of concrete is known to be sensitive to the degree of saturation and to chloride variations (Azarza and Gupta, 2017; Robles *et al*., 2022). The RC degradation process, partially controlled by the moving of aggressive ions through the concrete microstructure, leads to an increase in permeability (micro-fractures, cracks, concrete cover detachments), consequently exposing, to a greater extent, reinforcements to corrosion (Tuutti, 1982; Sbartaï *et al*., 2007; Du Plooy *et al*., 2013; Azarza and Gupta, 2017; Robles *et al*., 2022). Several studies have been conducted to determine the relationship between resistivity and corrosion risk, and to identify a resistivity threshold value where corrosion commences (Wong *et al*., 2019; Robles *et al*., 2022). This study presents the ERT investigations performed during the accelerated corrosion test. Lastly, the SP maps, acquired during the accelerated corrosion test with an unpolarisable electrode on the concrete sample surface, are also reported. The data collected with different NDT techniques (GPR, ERT, and SP) were used for an integrated analysis to define the evolution of the corrosion phenomenon on the reinforcement bar.

2. Materials and methods

2.1. RC laboratory samples

The sample was built with an ultra-fast setting cement compound comprising special binders, quartz and synthetic additives, which develops high mechanical strength in a very short time. The mechanical compressive strength after 28 days is greater than 2 N/mm^2. The mixture proportion is 1 kg of product per 22% of water. The concrete sample size is: length (l) = 500 mm, width (w) = 300 mm, and height (h) = 80 mm (Fig. 1a). The samples were constructed with an improved grip steel rebar, 10 mm in diameter and 350 mm long. The exposed length of the rebars is 25 mm per side. The concrete cover is 30 mm in the upper part of the sample and 40 mm in the lower part (Fig. 1).

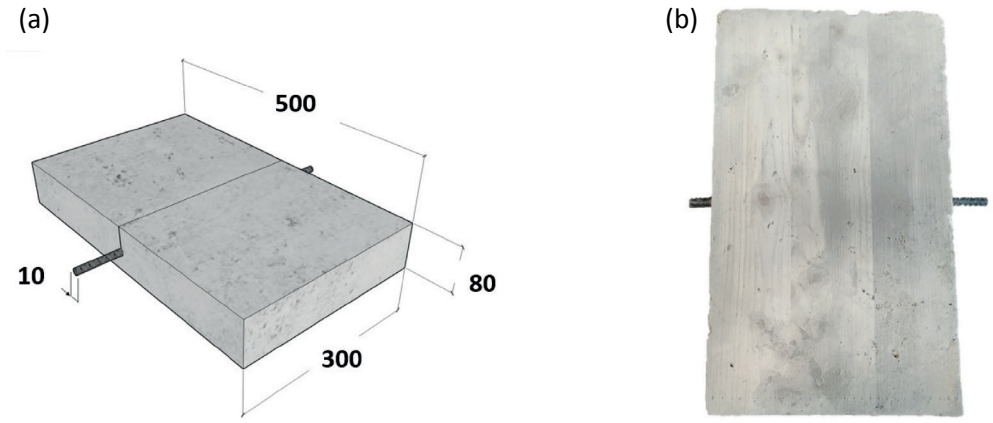

Fig. 1 - Sketch of the RC sample (a), with measurements given in millimetres. Top view of the RC sample complete with rebar (b).

A wooden box was used to build the concrete samples. The rebar was inserted inside the wooden box, into which concrete was, then, poured. After 30 days, the wooden box was removed and the concrete sample was ready (Fig. 1b). The NDT methods were applied during an experiment that can be divided into four phases:

- phase T1: sample in distilled water (5 surveys);
- phase T2: sample in water solution with 5% of sodium chloride (NaCl) (5 surveys);
- phase T3: sample during the accelerated corrosion test (10 surveys);
- phase T4: sample after the accelerated corrosion test (5 surveys).

During the first phase of this study, a RC sample was immersed in a plastic tank of distilled water. The experiment was set up to keep the tank water level constant at 10 mm from the bottom of the concrete sample throughout the investigation period. This was achieved with a refilling procedure.

The accelerated corrosion test was carried out by connecting the positive pole of a Hewlett DC power supply to the steel rebar (anode), and the negative pole was connected to a brass bar immersed in a water solution containing 5% of NaCl (cathode) (Fig. 2). The lower part of

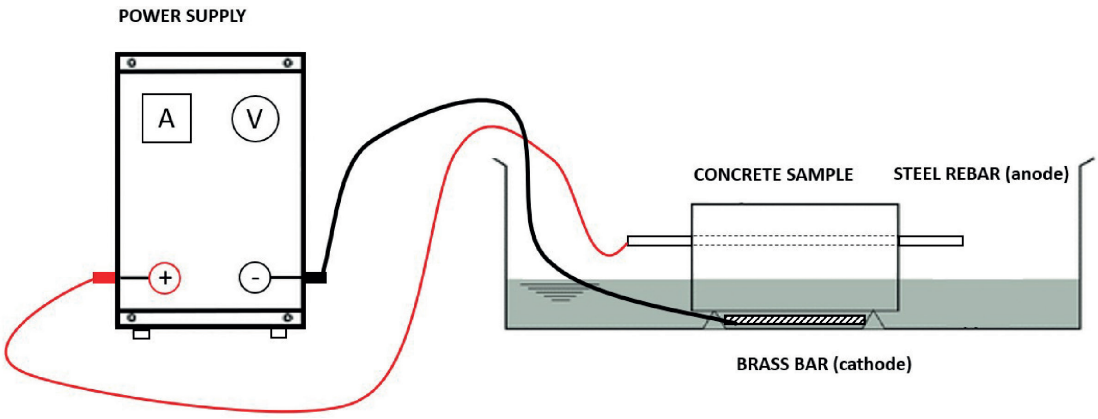

Fig. 2 - Sketch of the accelerated corrosion tests performed through the application of a power supply; the first centimetre of the RC sample was immersed in a water solution containing 5% of NaCl.

the concrete samples was immersed for 1 cm in a 5%-NaCl water solution. Through the DC power supply, a constant potential difference of 25.0 V was established. In the initial phase, the corrosion current was 0.4 A, then gradually lowered until it reached the minimum value of 0.08 A. The current was not constant, as the transmitter used only permitted a voltage adjustment. Nevertheless, during all the NDT (GPR, ERT, and SP) surveys, the DC power supply was switched off each time.

2.2. GPR acquisitions

One month after the construction of the concrete sample, GPR, ERT, and SP investigations were performed. The GPR dual antenna used was a 2-GHz antenna type GPR C-Thrue (IDS Geo-Radar s.r.l., Italy), with the following dimensions: 285 mm long, 200 mm wide, and 160 mm high. In order to cover the entire surface under investigation, a plexiglass support was built. Several parallel lines (totally 61), which would later be used in all acquisitions, were drawn with a line spacing of approximately 5 mm. To ensure all the radargrams were acquired with the same length (500 mm), an antenna stopper was installed as a start-line and end-line (Fig. 3).

The GPR acquisitions started at the bottom of the sample, following the first line drawn on the plexiglass, position 1 (Fig. 3). In this position, the front part of the GPR antenna is aligned with the edge of the concrete sample. The acquisition of the first radargram ends with the antenna in position 2 (Fig. 3). The GPR survey is completed with the acquisition of the last radargram

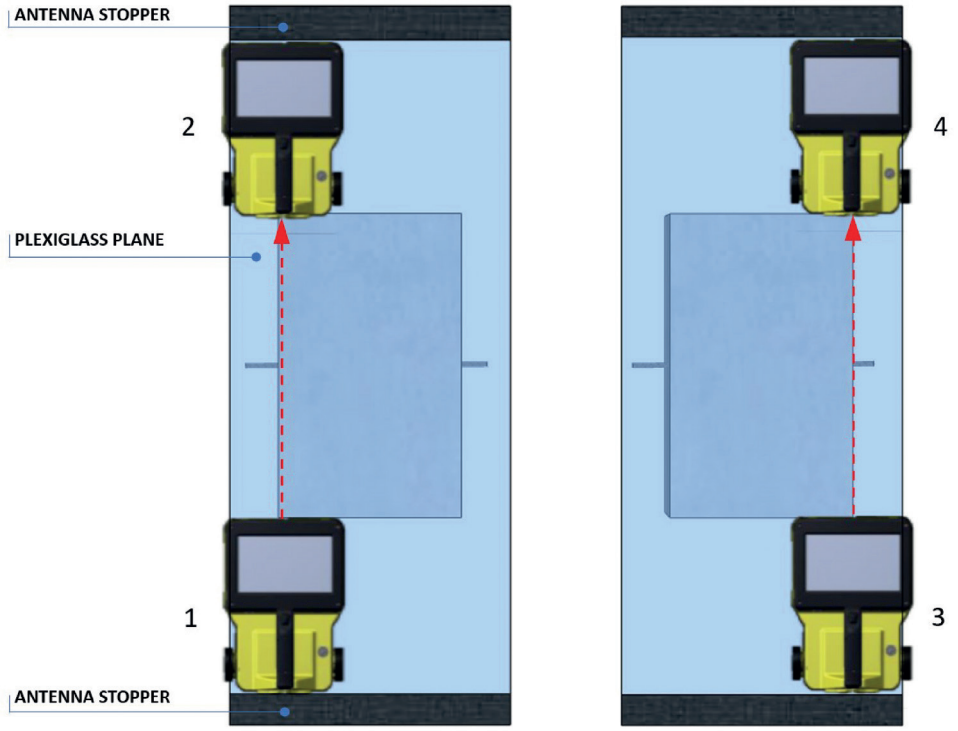

Fig. 3 - GPR acquisition system and plexiglass plane where the antenna stopper was installed to acquire radargrams of the same length and in the same position. The first radargram was acquired with the antenna starting in position 1 and ending in position 2. The last radargram (the 60th) was acquired with the antenna starting in position 3 and ending in position 4. The plexiglass surface is 120 × 50 cm^2.

(i.e. the 60th radargram) on the opposite edge of the sample, i.e. covering the entire 300-mm surface. The acquisition of the last radargrams starts in position 3 and ends in position 4 (Fig. 3). In this way, a complete data set of the concrete samples, under different conditions, was obtained before, during and after corroding the steel rebar (Table 1). Moreover, the trace distance taken into consideration was constant and set at 1.25 mm, and the number of samples per trace was 512.

Each radargram contains 400 traces (A-scans), while each survey comprises 24,400 traces (i.e. 61×400). In total, considering all the surveys conducted in the different phases, a total of 610,000 traces have been acquired on the concrete sample (Table 1). All the traces located over the rebar were extracted from each radargram, in order to implement the elaboration processing phase.

Table 1 - GPR acquired data set.

ID	No. surveys	No. radargrams	No. traces
Phase T1	5	305	122,000
Phase T2	5	305	122,000
Phase T3	10	610	244,000
Phase T4	5	305	122,000

The rebar in the middle of the concrete sample is located at 0.03 m (*S*) from the surface, and the corresponding two-way travel time (TWT) was measured at 0.6 ns (Fig. 6). Therefore, the *V (em sample)* is approximated to 0.10 m/ns by:

$$V(em\ sample) = \frac{S}{t} = \frac{S}{\left(\frac{TWT}{2}\right)} \quad (1)$$

and the relative dielectric permittivity ε of the sample is estimated in 9, by:

$$\varepsilon \text{ sample} = \frac{C^2}{[V(em\ sample)]^2} \quad (2)$$

where *C* is the speed of light in the vacuum.

2.3. ERT acquisitions

The Terrameter LS02 geo resistivity meter (ABEM Instrument, Sweden) was used for the ERT acquisitions on the concrete sample top surface, which was immersed in a 5% of NaCl water solution for 10-day corrosion test. The Abem Terrameter LS02 was connected to 24 steel nails, with 12 mm spacing. The steel nails, 50 mm long and 6 mm in diameter, were in direct contact with the sample surface and were connected to the cables by electrical clamps. A conductive gel was used to improve contact between the steel nails, used as electrodes, and the concrete sample. This setup enabled obtaining a resistance contact less than 0.3 KΩ. The acquisitions were obtained by arranging the electrodes perpendicularly to the reinforcing bar, in the central part of the concrete sample. Each day of the corrosion test, an ERT survey, with a dipole-dipole electrode configuration, was carried out (for a total of 10 ERT surveys).

Fig. 4 - Multi-electrode resistivity probe developed for ERT measurements. The ERT survey was acquired using the ABEM Terrameter LS02 instrument connected to 24 steel nails, acting as electrodes.

The ERTs were carried out during phase 3, when an accelerated corrosion test was performed. Once acquisition was completed, the data were downloaded with the Abem Terrameter LS Toolbox program. The apparent resistivity data were inverted using the ResIPy software (Rücker and Günther, 2011). ResIPy was developed to provide a more intuitive, and user-friendly, approach for the inversion of geoelectrical data, by using an open-source graphical user interface and a Python application programming interface (Capozzoli *et al*., 2021). The software utilises the R2/R3t inversion codes for apparent electrical resistivity data inversion based on the widely used Occam approach of DeGroot-Hedlin and Constable (De Groot-Hedlin and Constable, 1990; Capozzoli *et al*., 2021). The earth is discretised into a series of blocks, each containing one or more elements. The Occam inversion finds the smoothest 2D model for which the chi-squared statistic equals an *a priori* value (Binley, 2015).

2.4. SP acquisitions

During the corrosion test, SP acquisitions were carried out on the sample immersed in a water solution containing 5% of NaCl. The SP measurement on the sample consists in the acquisition of the electric potential (mV) between the rebar and the reference electrode in contact with the cement surface. This method defines the corrosion potential level of the rebar structure (ASTM C876-91, 1999; Pour-Ghaz *et al*., 2009; ASTM C876-15, 2015).

To ensure the measurements were always obtained from the same investigation points, the electrodes were fitted into a wooden frame, with 54 equally-distanced drilled holes, covering the entire surface of the concrete sample (Fig. 5). The unpolarisable electrode (Pb-$PbCl_2$ type) was

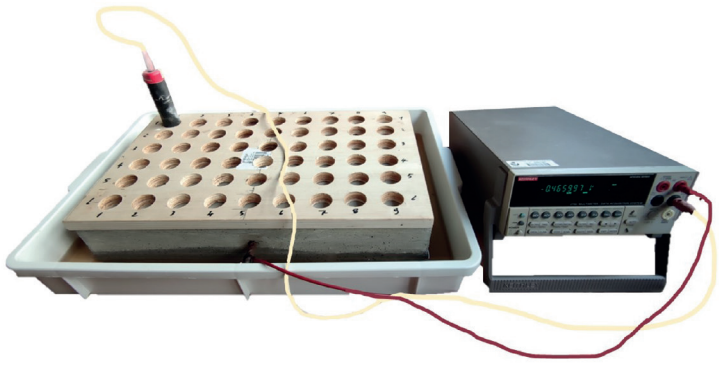

Fig. 5 - SP acquisitions on the RC sample (Fornasari *et al*., 2023).

connected to the Keithley multimeter at high impedance, while the positive pole was connected to the armature bar.

3. Results

3.1. GPR processing and results

The radargrams acquired were processed with Reflex-W (Sandmeier, 2016), using the Hilbert transform to calculate the trace envelope. All the processed GPR data were exported and analysed with *ad-hoc* script, enabling obtaining the single traces of the radargram in correspondence of the rebar placed precisely in the middle of the sample. The traces analysed correspond to the traces at the top of the rebar (Fig. 6).

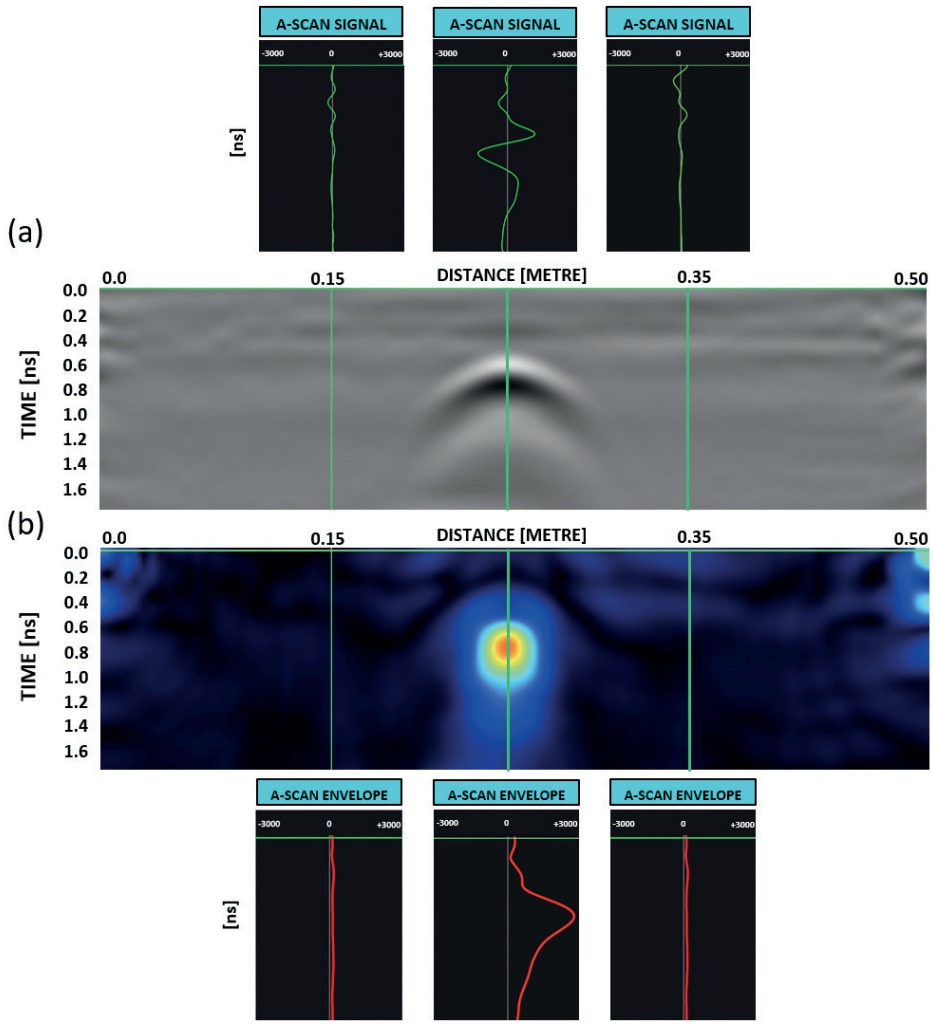

Fig. 6 - One of the radargrams acquired at the centre of the concrete sample. In the radargram in panel a, the traces are shown 10 cm before the steel reinforcing bar, on the steel reinforcing bar, and 10 cm after the steel reinforcing bar. The radargram in panel a shows the trace amplitude; the radargram in panel b shows the trace envelope.

The process described enabled analysing the variation of the envelope attribute of the trace located on the top of the rebar for phase T1, when the sample was immersed in distilled water, for phase T2, when the sample was immersed in water with 5% of NaCl, for phase T3, when the steel rebar inside the concrete sample was subjected to the accelerated corrosion test, and for phase T4, after the switch off of the power supply used for the accelerated corrosion test. The processing phase consisted in extracting the envelope values from the traces acquired on the rebar position, located at 0.6 ns (at a depth of 30 mm). Next, all the envelope values, resulting from all the experimental phases, were compared (Fig. 7). During phase T1, five peaks of the envelope A-scan were depicted, highlighting a constant value of approximately 2,800.

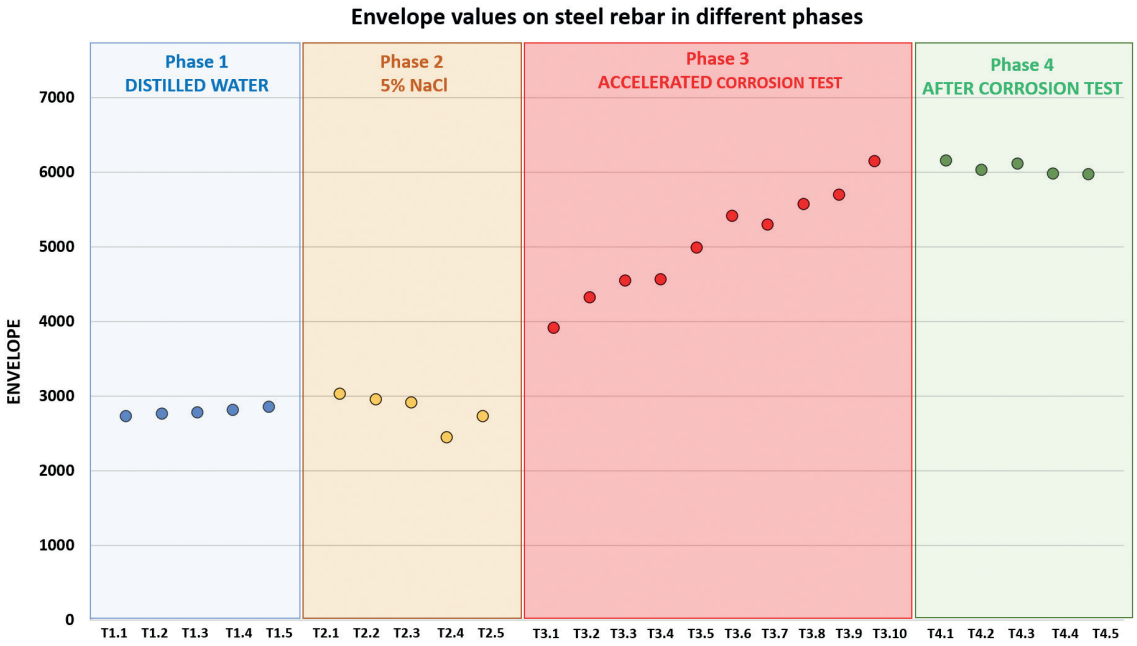

Fig. 7 - The envelope values are all obtained from an A-scan acquired on position no. 29, i.e. exactly in the middle of the concrete sample over the steel rebar at 0.6 ns. Phase 1 shows an almost constant envelope value during the five days of investigation (T1_1 to T1_5). In phase 2, the concrete sample was immersed in a 5%-NaCl water solution, and small variations of the envelope values were identified. In phase 3, the envelope values were acquired during the accelerated corrosion test, during which they showed an increase every 24 hours. In phase 4, the corrosion test was turned off. The maximum envelope value, reached on the last day of the corrosion test (T3_10), is observed to maintain an almost constant value during the following days.

During phase T2, the concrete sample was immersed in salt water with 5% of NaCl; the GPR investigations, on the concrete samples, began only after 10 days. This delay time was defined to allow the triggered corrosion phenomena, due to chloride on the steel rebar, to occur. After such delay time, five envelope values were extracted from the radargrams acquired during the five consecutive days. The envelope values of phase T2 are greater than those of the previous phase. On the contrary, a small variation in the envelope values was identified with the data acquired at section T2_4. This outlier was associated with the presence of higher humidity on the shallow surface that decreased the envelope values on that day. This phenomenon was also observed during the following phases, when small decreases of the envelope trend were highlighted.

During induced corrosion (phase T3), an increase of the envelope value was observed (from 4,000 to 6,200). Moreover, in order to check the quality of the proposed process to detect the corrosion phenomena, two different traces on the same radargrams, but located in different positions, were extracted during each day. The two new A-scans were localised 10 cm symmetrically away from the location of the reinforcing bar (Fig. 8), where the previous analysed traces were located. Their positions were defined to avoid the interference both with the steel rebar reflection and with the sample edges. Fig. 8 depicts the three different envelope trend values transmitted by the three different A-scan signals. The envelope values, obtained from the traces far from the rebar, highlight a constant trend during the induced corrosion test. On the contrary, the envelope values on the rebar depict a marked variation due to corrosion phenomena (Fig. 8).

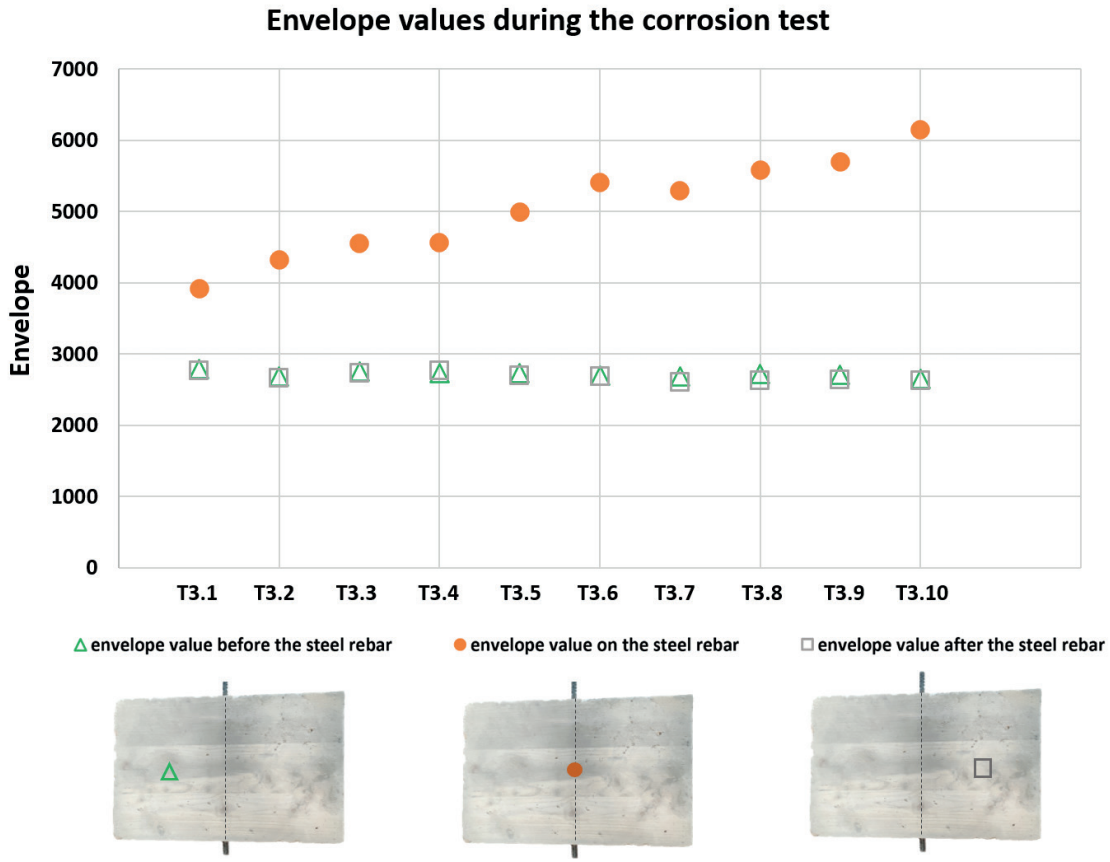

Fig. 8 - The diagram displays the envelope values taken from the radargram conducted in the midpoint of the sample and perpendicularly to the reinforcing bar during the corrosion test. The envelope values were taken at 0.6 ns, specifically on the envelope A-scan trace at 10 cm from the rebar location, in symmetrical positions from it (green triangle and grey square), and above the reinforcing bar (orange dot). An increase in the envelope attribute is observed during the corrosion test only on the reinforcing bar (orange dot).

After 10 days of accelerated corrosion test, the current supply was stopped, and GPR data were acquired for another 5 days (phase T4). The processed data of phase T4 show almost constant envelope values (around 6,000).

3.2. ERT processing and results

The results of the investigations carried out on the rebar inside the concrete sample, during the accelerated corrosion test, were acquired every day, and were processed in timelapse. The resistivity data were processed following the ResIPy protocol. The mesh utilised was a triangular-shaped mesh, and the data were sent to the inversion pipeline, where the resulting inverted section was produced with a diagnostic pseudo-section of the normalised inversion error. With such method, it was possible to determine resistivity at different levels/depths in order to reconstruct the spatial distribution of material resistivity (Hubbard *et al.*, 2003). Fig. 9 shows all the inverted electrical resistivity tomography measurements acquired during the induced corrosion phase (phase T3). The reinforcement bar was placed between electrode 12 and electrode 13, at a depth from the surface of approximately 0.03 m. The ERT T3_1 section was acquired 24 hours after the start of the steel rebar corrosion test. The following ERT sections (T3_2, T3_3, T3_4, T3_5, T3_6, T3_7, T3_8, T3_9, and T3_10) were acquired every day. In the first ERT section acquired (T3_1), the resistivity values are rather low (less than 20 Ωm) and homogeneous. The low resistivity values on the cement sample can be explained by the fact

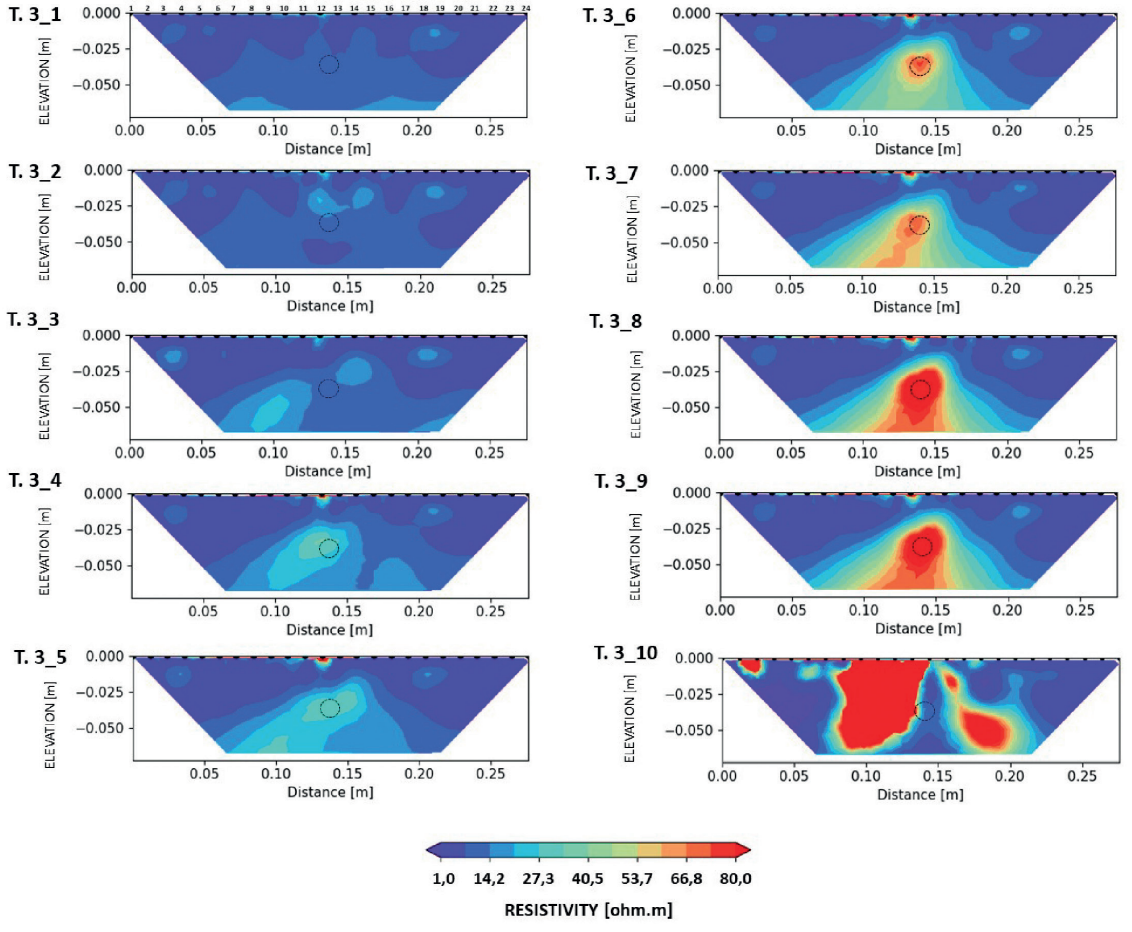

Fig. 9 - The reported sections were obtained during the corrosion test. Section T3_1 was obtained 24 hours after the start of the accelerated corrosion test, and section T3_10 after 10 days of testing. The position of the steel rebar is identified by the black dashed circle.

that the sample is immersed in water with 5% of NaCl. The concrete sample utilised has very high porosity that facilitates the penetration of the solution, thus making the concrete more conductive. With an increase of the rebar corrosion, the ERT sections highlight a progressive increase in the resistivity values in the central part of the section, exactly in correspondence of the steel rebar. This behaviour should be associated with a degradation of the cement around the rebar due to the rust zone, probably due to mineral phase changing. During the induced corrosion phase, the resistivity anomaly expanded, defining an increase of the rust zone around the rebar. Moreover, the resistivity anomaly of the T.3_10 tomography highlighted a large resistivity zone probably due to cracks inside the sample.

3.3. SP processing and analysis

SP investigations were carried out every day on the RC sample partially immersed in a water solution with 5% of NaCl, and during the accelerated corrosion tests for 10 days (phase T3). The SP measurements were carried out prior to the ERT acquisition.

The procedure adopted consisted in measuring the electric potential difference between the steel rebar and a reference electrode (in this case, an unpolarisable lead electrode was used). The reference electrode was placed in direct contact with the sample surface, and the negative cable was connected to a voltmeter, while the reinforcement bar was connected to the positive pole. The acquired data enabled mapping the isopotential lines using the Surfer software (Fig. 10). The isopotential lines highlight the presence of corrosion phenomena in progress at the time of the measurement. The colour scale used ranges from white (low values) to red (high values). Low potential values (less than 300 mV) suggest a passive state of the rebar with no corrosion phenomena in progress. Potential values greater than 300 mV define the corrosion trigger. The steel rebar position is identified on the SP maps with a black dotted line (Fig. 10). By observing the SP maps after 24 hours of activated corrosion test (T3_1), the potential values result to be approximately 120-140 mV. The highest potential values in the T3_1 map are shown on the left side of the steel rebar (180 mV). In the successive SP maps, taken every 24 hours during the corrosion test, the values generally increase on the entire surface of the concrete sample. The T3_10 isopotential map, acquired after 10 days of corrosion tests, shows potential values above 500 mV. The highest values are recorded at the rebar location, i.e. on the edges of the concrete sample. In this zone, there are two red areas (high potential) that should be associated with the highest corroded zone. Even if this method is able to detect corrosion, the electrical potential presents a volumetric behaviour that is caused by a chemical process; therefore, its variations are clearly observable on the entire surface of the sample.

4. Discussion and conclusions

In this article, an experimental setup was designed to simulate an accelerated corrosion process on a cement sample, and to monitor the effect of steel rebar corrosion by means of NDT applications. In detail, in the presence of increasing corrosion, the experiment highlighted an increase of the GPR envelope attribute and a variation of the signal acquired by the ERT and SP methods. The use of these three methods on an induced corrosion experiment is still quite novel, and, in fact, only a limited number of studies have been conducted to this day (Tešic' *et al*., 2021).

A certain number of previous studies regarding GPR applications, performed to observe controlled corrosion experiments, describe discrepant results; indeed, while some authors

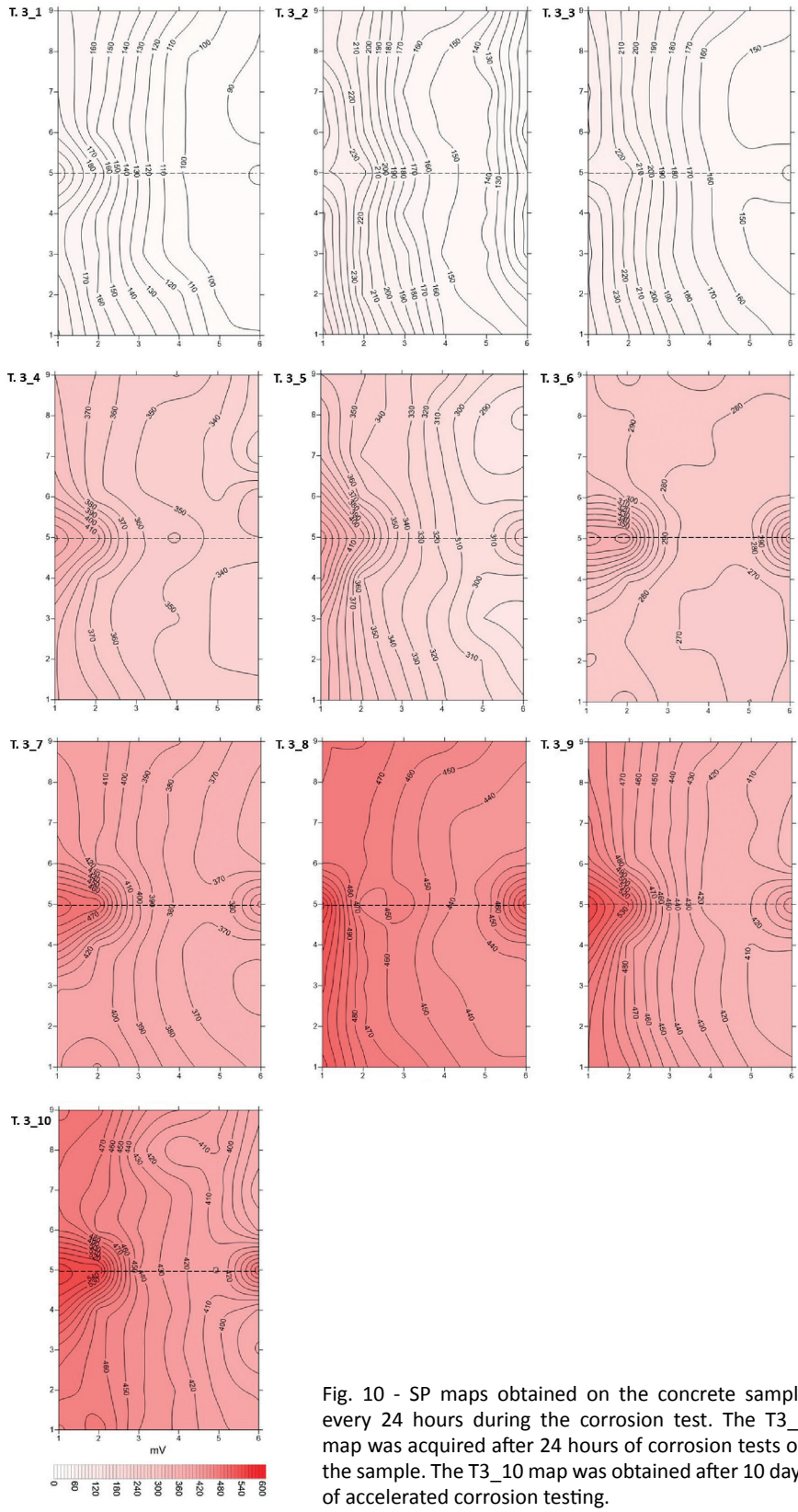

Fig. 10 - SP maps obtained on the concrete sample every 24 hours during the corrosion test. The T3_1 map was acquired after 24 hours of corrosion tests on the sample. The T3_10 map was obtained after 10 days of accelerated corrosion testing.

observe an increase in the signal amplitude trace during corrosion (Hubbard *et al*., 2003; Zaki *et al*., 2018; Sossa *et al*., 2019), others observe a decrease in the amplitude trace after steel rebar corrosion (Lai *et al*., 2010, 2011, 2013; Raju *et al*., 2018). The different results obtained are due to the lack of a common line in the execution of the tests in terms of experimental setup, choice of cement, quantity of chlorides, corrosion level, and induced damage. Some researchers carry out tests before and after the corrosion phase (Hubbard *et al*., 2003; Lai *et al*., 2010; Raju *et al*., 2018; Zaki *et al*., 2018; Sossa *et al*., 2019), while only a few do so throughout the entire corrosion test (Lai *et al*., 2011, 2013; Raju *et al*., 2018). From the point of view of the authors, the corrosion phenomena need a monitoring approach, and only an acceleration corrosion process should be analysed through dedicated NDT experiments (Tešic' *et al*., 2021). Moreover, the described results highlight that a multisensor approach can improve the quality of corrosion diagnosis of steel rebars on concrete structures. Indeed, the experiments performed highlight the importance of integrating the different NDT methods. During the induced corrosion phase (phase T3), an increase of the envelope values in the GPR data was observed and, concurrently, the SP and resistivity values also increased. Initially, the resistivity values of the investigated sample showed low values (less than 20 Ωm) and, therefore, the sample plausibly prone to heavy corrosion, as similarly described by Robles *et al*. (2022). On the contrary, during the accelerated corrosion test, an increase in the resistivity of the concrete sample is observed (greater than 70 Ωm). This behaviour is due to the presence of concrete degradation and induced cracks during the formation of corrosion (Rodrigues *et al*., 2021).

The static potential values could be an indicator of the condition of the corrosion in the embedded reinforcing bars. On the contrary, rebar corrosion is observed on the concrete surface in large potential gradients that can readily be located in isopotential contour maps obtained from the survey results. Therefore, the laboratory experiments enabled defining the main characteristics of the NDT methods applied, thus, highlighting the usefulness of each method in monitoring (e.g. ERT and GPR), or in achieving a static characterisation (e.g. SP). However, SP is useful in conducting preliminary screening on concrete structures, and identifying areas where the corrosion phenomena are ongoing. In order to obtain more detailed information, ERT is important in determining quality control and performance assessments of concrete material, while GPR is able to obtain localised information on reinforcing bar corrosion.

It should be noted that on-site conditions can introduce anisotropy caused, for instance, by different moisture and chloride contents, which may lead to an ambiguous detection of the corroded zones when based only on a single point observation. For this reason, it is necessary to detect different physical parameters associated with the corrosive environment housing the steel rebar. Nevertheless, new controlled tests, exploiting a combination of NDT techniques with a multisensor approach (such as SP, direct current, induced polarisation, infrared thermography, and ultrasonic) will be of crucial importance. Future steps will involve samples with an increased number of rebars and more complex rebar configurations to simulate more realistic scenarios.

REFERENCES

ASTM C876-91; 1999: *Standard test method for half-cell potentials of uncoated reinforcing steel in concrete.* American Society for Testing and Materials International, West Conshohocken, PA, USA.

ASTM C876-15; 2015: *Standard test method for corrosion potentials of uncoated reinforcing steel in concrete*. American Society for Testing and Materials International, West Conshohocken, PA, USA.

Azarza P. and Gupta R.; 2017: *Electrical resistivity of concrete for durability evaluation: a review.* Adv. Mater. Sci. Eng., 8453095, 30 pp., doi: 10.1155/2017/8453095.

Binley A.; 2015: *Tools and techniques: DC electrical methods.* In: Schubert G. (ed), Treatise on Geophysics 2nd ed., Elsevier, New York, NY, USA, pp. 233-259.

Bossio A., Monetta T., Bellucci F., Lignola G.P. and Prota A.; 2015: *Modelling of concrete cracking due to corrosion process of reinforcement bars.* Cem. Concr. Res., 71, 78-92, doi: 10.1016/j.cemconres.2015.01.010.

Capozzoli L. and Rizzo E.; 2017: *Combined NDT techniques in civil engineering applications: laboratory and real test.* Constr. Build. Mater., 154, 1139-1150, doi: 10.1016/j.conbuildmat.2017.07.147.

Capozzoli L., Fornasari G., Giampaolo V., De Martino G. and Rizzo E.; 2021: *Multi-sensors geophysical monitoring for reinforced concrete engineering structures: a laboratory test.* Sens., 21, 5565, 22 pp., doi: 10.3390/s21165565.

Chang C.W., Tsai C.A. and Shiau Y.C.; 2022: *Inspection of steel bars corrosion in reinforced concrete structures by non-destructive Ground Penetrating Radar.* Appl. Sci., 12, 5567, 18 pp., doi: 10.3390/app12115567.

Daniyal M. and Akhtar S.; 2020: *Corrosion assessment and control techniques for reinforced concrete.* J. Build. Pathol. Rehabil., 5, 1-20, doi: 10.1007/s41024-019-0067-3.

De Groot-Hedlin C. and Constable S.; 1990: *Occam's inversion to generate smooth, two-dimensional models from magnetotelluric data.* Geophys., 55, 1613-1624, doi: 10.1190/1.3581356.

Duffó G.S., Reinoso M., Ramos C.P. and Farina S.B.; 2012: *Characterization of steel rebars embedded in a 70-year old concrete structure.* Cement and Concrete Research, 42, 111-117, doi 10.1016/j.cemconres.2011.08.003.

Du Plooy R., Palma Lopes S., Villain G. and Dérobert X.; 2013: *Development of a multi-ring resistivity cell and multi-electrode resistivity probe for investigation of cover.* NDT and E Int., 54, 27-36, doi: 10.1016/j.ndteint.2012.11.007.

Fornasari G., Capozzoli L., De Martino M., Giampaolo V. and Rizzo E.; 2022: *Rebar corrosion monitoring with a multisensor non-destructive geophysical techniques.* In: Proc. 45th International Conference on Telecommunications and Signal Processing (TSP), Prague, Czech Republic, pp. 367-370, doi: 10.1109/TSP55681.2022.9851352.

Fornasari G., Capozzoli L. and Rizzo E.; 2023: *Combined GPR and self-potential techniques for monitoring steel rebar corrosion in reinforced concrete structures: a laboratory study.* Remote Sens., 15, 2206, 18 pp., doi: 10.3390/rs15082206.

Hong S., Lai W.W.L., Wilsch G., Helmerich R., Helmerich R., Günther T. and Wiggenhauser H.; 2014: *Periodic mapping of reinforcement corrosion in intrusive chloride contaminated concrete with GPR.* Construct. Build. Mater., 66, 671-684, doi: 10.1016/j.conbuildmat.2014.06.019.

Hong S., Lai W.W.L. and Helmerich R.; 2015: *Experimental monitoring of chloride-induced reinforcement corrosion and chloride contamination in concrete with Ground-Penetrating Radar.* Struct. Infrastruct. Eng., 11, 15-26, doi: 10.1080/15732479.2013.879321.

Hornbostel K., Larsen C.K. and Geiker M.R.; 2013: *Relationship between concrete resistivity and corrosion rate – A literature review.* Cem. Concr. Compos., 39, 60-72, doi: 10.1016/j.cemconcomp.2013.03.019.

Hubbard S.S., Zhang J., Monteiro P.J.M., Peterson J.E. and Rubin Y.; 2003: *Experimental detection of reinforcing bar corrosion using non-destructive geophysical techniques.* ACI Mater. J., 100, 501-510, doi: 10.14359/12957.

Lai W.W.L., Kind T. and Wiggenhauser H.; 2010: *Detection of accelerated reinforcement corrosion in concrete by Ground Penetrating Radar.* In: Proc. XIII International Conference on Ground Penetrating Radar, Lecce, Italy, pp. 1-5, doi: 10.1109/ICGPR.2010.5550254.

Lai W.W.L., Kind T. and Wiggenhauser H.; 2011: *Using Ground Penetrating Radar and time-frequency analysis to characterize construction materials.* NDT and E Int., 44, 111-120, doi: 10.1016/j.ndteint.2010.10.002.

Lai W.W.L., Kind T., Stoppel M. and Wiggenhauser H.; 2013: *Measurement of accelerated steel corrosion in concrete using Ground Penetrating Radar and a modified half-cell potential method.* J. Infrastruct. Syst., 19, 205-220, doi: 10.1061/(ASCE)IS.1943-555X.0000083.

Ohtsu M.; 2016: *Introduction*. In: Ohtsu M. (ed), Innovative AE and NDT Techniques for On-Site Measurement of Concrete and Masonry Structures, State-of-the-Art Report of the RILEM Technical Committee 239-MCM, Springer, Berlin, Germany, pp. 1-4.

Ormellese M., Berra M., Bolzoni F. and Pastore T.; 2006: *Corrosion inhibitors for chlorides induced corrosion in reinforced concrete structures.* Cem. Concr. Compos., 36, 536-547, doi: 10.1016/j.cemconres.2005.11.007.

Pacheco-Torgal F., Melchers R.E., Shi X., De Belie N., Van Tittelboom K. and Sáez A.; 2018: *Eco-efficient repair and rehabilitation of concrete infrastructures.* Elsevier, Woodhead, Oxford, UK, 777 pp., doi: 10.1016/C2016-0-04100-1.

Pour-Ghaz M., Isgor O.B. and Ghods P.; 2009: *Quantitative interpretation of half-cell potential measurements in concrete structures.* J. Mat. Civ. Eng., 21, 467-475, doi: 10.1061/(ASCE)0899-1561(2009)21:9(467).

Raju R.K., Hasan M.I. and Yazdani N.; 2018: *Quantitative relationship involving reinforcing bar corrosion and Ground-Penetrating Radar amplitude.* ACI Mater. J., 115, 449-457, doi: 10.14359/51702187.

Ramezanianpour A.A., Pilvar A., Mahdikhani M. and Moodi F.; 2011: *Practical evaluation of relationship between concrete resistivity, water penetration, rapid chloride penetration and compressive strength.* Constr. Build. Mater., 25, 2472-2479, doi: 10.1016/j.conbuildmat.2010.11.069.

Robles K.P., Yee J.J. and Kee S.H.; 2022: *Electrical resistivity measurements for non-destructive evaluation of chloride-induced deterioration of reinforced concrete — A review.* Mater., 15, 2725, 31 pp., doi: 10.3390/ma15082725.

Rodrigues R., Gaboreau S., Gance J., Ignatiadis I. and Betelu S.; 2021: *Reinforced concrete structures: a review of corrosion mechanisms and advances in electrical methods for corrosion monitoring.* Constr. Build. Mater., 269, 121240, 82 pp., doi: 10.1016/j.conbuildmat.2020.121240.

Rücker C. and Günther T.; 2011: *The simulation of finite ERT electrodes using the complete electrode model.* Geophys., 76, 227-238, doi: 10.1190/1.3581356.

Sandmeier K.J.; 2016: *ReflexW Version 8.1. Program for processing of seismic, acoustic or electromagnetic reflection, refraction and transmission data. Software manual*. Karlsruhe, Germany, 628 pp.

Sbartaï Z.M., Laurens S., Rhazi J., Balayssac J.P. and Arliguie G.; 2007: *Using radar direct wave for concrete condition assessment: correlation with electrical resistivity.* J. Appl. Geophys., 62, 361-374, doi: 10.1016/j.jappgeo.2007.02.003.

Shevtsov D., Cao N.L., Nguyen V.C., Nong Q.Q., Le H.Q., Nguyen D.A., Zartsyn I. and Kozaderov O.; 2022: *Progress in sensors for monitoring reinforcement corrosion in reinforced concrete structures — A review.* Sens., 22, 3421, 24 pp., doi: 10.3390/s22093421.

Sossa V., Pérez-Gracia V., González-Drigo R. and Rasol M.A.; 2019: *Lab non-destructive test to analyze the effect of corrosion on Ground Penetrating Radar scans.* Remote Sens., 11, 2814, 15 pp., doi: 10.3390/rs11232814.

Tešic' K., Baricevic A. and Serdar M.; 2021: *Non-destructive corrosion inspection of reinforced concrete using Ground-Penetrating Radar: a review.* Mater., 14, 975, 20 pp., doi: 10.3390/ma14040975.

Tešic' K.; Baricevic A., Serdar M. and Gucunski N.; 2022: *Characterization of ground penetrating radar signal during simulated corrosion of concrete reinforcement.* Autom. Constr., 143, 13 pp., doi: 10.1016/j.autcon.2022.104548.

Tosti F., Alani A.M. and Benedetto A.; 2020: *Guest editorial: recent advances in non-destructive testing methods.* Surv. Geophys., 41, 365-369, doi: 10.1007/s10712-020-09592-7.

Tuutti K.; 1982: *Corrosion of steel in concrete.* Doctoral Thesis (monograph), Division of Building Materials, Swedish Cement and Concrete Research Institute, Stockholm, Sweden, 469 pp.

Venkatesan P., Rajendran A., Srinivasan S. and Kannan S.; 2003: *Corrosion of reinforced concrete exposed to marine atmosphere.* Trans. Soc. Adv. Electrochem. Sci. Technol., 38, 53-56.

Verma S.K., Bhadauria S.S. and Akhtar S.; 2014: *Monitoring corrosion of steel bars in reinforced concrete structures.* Sci. World J., 957904, 9 pp., doi: 10.1155/2014/957904.

Wong P.T.W., Lai W.W.L., Sham J.F.C. and Poon C.; 2019: *Hybrid non-destructive evaluation methods for characterizing chloride-induced corrosion in concrete.* NDT and E Int., 107, 102123, **?? pp.,** doi: 10.1016/j.ndteint.2019.05.008.

Zaki A., Chai K.H., Aggelis G.D. and Alver N.; 2015: *Non-destructive evaluation for corrosion monitoring in concrete: a review and capability of acoustic emission technique.* Sens., 15, 19069-19101, doi: 10.3390/s150819069.

Zaki A., Johari M.A., Hussin W.M.A.W. and Jusman Y.; 2018: *Experimental assessment of rebar corrosion in concrete slab using Ground Penetrating Radar (GPR).* Int. J: Corros., ID 5389829, 10 pp., doi: 10.1155/2018/5389829.

Corresponding author: Giacomo Fornasari
Dip. Fisica e Scienze della Terra, Università degli Studi di Ferrara
Via Saragat 1, 44123 Ferrara, Italy
Phone: +39 333 356 6026; e-mail: giacomo.fornasari@unife.it